Journal of Alzheimer's Disease 62 (2018) 1595–1607
DOI 10.3233/JAD-170582
IOS Press

[^{18}F]-Flutemetamol Uptake in Cortex and White Matter: Comparison with Cerebrospinal Fluid Biomarkers and [^{18}F]-Fludeoxyglucose

Lisa Flem Kalheim[a,c,*], Tormod Fladby[a,c], Christopher Coello[d], Atle Bjørnerud[b] and Per Selnes[a,c]
[a]*Department of Neurology, Akershus University Hospital, Lørenskog, Norway*
[b]*The Intervention Centre, Oslo University Hospital, Oslo, Norway*
[c]*Institute of Clinical Medicine, Campus Ahus, University of Oslo, Oslo, Norway*
[d]*Preclinical PET/CT, Institute of Basic Medical Sciences, University of Oslo, Oslo, Norway*

Handling Associate Editor: Andrea Chincarini

Accepted 3 January 2018

Abstract. Flutemetamol (^{18}F-Flut) is an [^{18}F]-labelled amyloid PET tracer with increasing availability. The main objectives of this study were to investigate 1) cerebrospinal fluid (CSF) Aβ 1-42 ($A\beta_{42}$) concentrations associated with regional ^{18}F-Flut uptake, 2) associations between cortical ^{18}F-Flut and [^{18}F]-fludeoxyglucose (^{18}F-FDG)-PET, and 3) the potential use of ^{18}F-Flut in WM pathology. Cognitively impaired, nondemented subjects were recruited ($n = 44$). CSF was drawn, and ^{18}F-Flut-PET, ^{18}F-FDG-PET, and MRI performed. Our main findings were: 1) Different Alzheimer's disease predilection areas showed increased ^{18}F-Flut retention at different CSF $A\beta_{42}$ concentrations (posterior regions were involved at higher concentrations). 2) There were strong negative correlations between regional cortical ^{18}F-Flut and ^{18}F-FDG uptake. 3) Increased ^{18}F-Flut uptake were observed in multiple subcortical regions in amyloid positive subjects, including investigated reference regions. However, WM hyperintensity ^{18}F-Flut standardized uptake value ratios (SUVr) were not significantly different, thus we cannot definitely conclude that the higher uptake in ^{18}F-Flut(+) is due to amyloid deposition. In conclusion, our findings support clinical use of CSF $A\beta_{42}$, putatively relate decreasing CSF $A\beta_{42}$ concentrations to a sequence of regional amyloid deposition, and associate amyloid pathology to cortical hypometabolism. However, we cannot conclude that ^{18}F-Flut-PET is a suitable marker for WM pathology due to high aberrant WM uptake.

Keywords: Alzheimer's disease, cerebrospinal fluid, imaging, positron emission tomography, white matter disease

INTRODUCTION

Aggregation and deposition of amyloid-β peptides (Aβ) into plaques is considered a key event in the evolution of Alzheimer's disease (AD) [1]. There are two types of amyloid biomarkers: assays to measure cerebrospinal fluid (CSF) Aβ 1-42 ($A\beta_{42}$) and PET tracers binding amyloid. Both reliably identify amyloid plaque deposition [2] and show high concordance in diagnosing AD [3, 4]. They are thus considered equal markers of brain amyloidosis [5], but discrepancies occur [4, 6], demonstrated by, for example, abnormal CSF $A\beta_{42}$ and negative PET or vice versa. CSF $A\beta_{42}$ becomes decreased (or pathological) before amyloid PET, as PET tracers bind strongly to fibrillar Aβ and less strongly to diffuse Aβ

*Correspondence to: Lisa Flem Kalheim, Department of Neurology, Akershus University Hospital, PO. Box 1000, 1478 Lørenskog, Norway. Tel.: +0047 98035050; E-mail: Lisa.Flem.Kalheim@ahus.no.

ISSN 1387-2877/18/$35.00

plaques [7]. Other possible explanations are inconsistencies in amyloid PET rating, incorrect handling or between-laboratory and batch-to-batch CSF assay variability, a known issue for these analyses [8]. Hence standardization is important for correct detection of incipient AD. We have insufficient knowledge about at which CSF $A\beta_{42}$ concentrations amyloid PET becomes abnormal, and in which areas this happens first. CSF analyses are likely more available, and such knowledge may improve the diagnostic accuracy of CSF $A\beta_{42}$ also to predict regional deposition at different CSF $A\beta_{42}$ concentrations.

[^{11}C] Pittsburgh compound B (^{11}C-PiB) [9] is widely investigated, but ^{18}F-labelled amyloid radiotracers (with increased availability due to longer half-life) have more recently been developed. Herein, we investigate [^{18}F]-Flutemetamol (^{18}F-Flut) [10] (a structural analogue to ^{11}C-PiB). ^{11}C-PiB and ^{18}F-Flut are comparable with respect to cortical retention, but ^{18}F-Flut typically presents with higher white matter (WM) uptake [11]. Possible explanations for the higher WM ^{18}F-Flut uptake include non-specific uptake related to lipophilicity [12] in the high lipid content WM, and aberrant binding to the β-sheet structured myelin basic protein [13]. ^{18}F-Flut clearance is also slower in WM compared to grey matter (GM) [14].

^{18}F-Flut WM retention may pose challenges due to partial volume effects (PVE) (i.e., spill-over from areas of high uptake to adjacent areas of low uptake) [15]. It is not clear to which extent WM ^{18}F-Flut uptake depends on pathology (e.g., WM amyloid load or pathology of the capillary bed) or is aberrant and unspecific, warranting further investigation of ^{18}F-Flut for use in WM.

Applying PVE correction (PVC) enhances quantitative accuracy of ^{18}F-Flut PET [15], and may also avoid bias in WM analyses. PVC may optimize PET images for studies of WM function and pathology, as we recently demonstrated with [^{18}F]-fluorodeoxyglucose PET (FDG-PET) [16] (and also with diffusion tensor imaging [17]).

White matter hyperintensities of presumed vascular origin (WMHs) [18] (as visualized on T2-weighted MRI images) are thought to reflect underlying small-vessel cerebrovascular disease (CVD) [18]. There is strong evidence for an association between CVD and AD [19], but it is not certain whether there is a pathomechanistic interaction, or whether CVD is an independent process with manifestations like hippocampal atrophy [20] and synergistic effects on the clinical symptoms of AD. In both AD and CVD [21], there are microvascular alterations with capillary dysfunction, and the neurovascular unit is affected, impairing the blood-brain barrier and clearance of soluble substances [22, 23], and even amyloid deposits may be located at the outer basement membrane (cerebral amyloid angiopathy (CAA) type 1 [24]).

Establishing the potential contribution of amyloid pathology to vascular alterations (or vice versa) seen in AD may be of diagnostic, preventive and therapeutic value. To date, a handful studies have applied ^{11}C-PiB to analyses of WM, showing reduced retention in WMHs compared to normal-appearing WM (NAWM) [25–27]. ^{11}C-PiB is also shown to label vascular amyloid depositions [28, 29] as well as cortical deposits, a feature that may also be attributable to ^{18}F-Flut given their structural similarities. WM ^{18}F-Flut binding has been characterized [13], but to the best of our knowledge use of ^{18}F-Flut in WMH has not been examined.

The objectives of the current study were therefore 1) to compare CSF $A\beta_{42}$ and ^{18}F-Flut uptake to evaluate the different Aβ concentrations at which regional ^{18}F-Flut uptake becomes abnormal, 2) to investigate associations between cortical ^{18}F-Flut and ^{18}F-FDG uptake, and 3) to investigate the potential use of ^{18}F-Flut in analyses of WM pathology. For comparative purposes, we analyzed ^{18}F-Flut uptake in different reference regions, regions not prone to plaque deposition, and also compared subcortical retention in subjects classified as ^{18}F-Flut positive and ^{18}F-Flut negative to investigate potential contribution of amyloid dysmetabolism to WM pathology in AD.

MATERIAL AND METHODS

Subjects

Forty-eight subjects were included from a longitudinal cohort followed at a university hospital from 2013 to 2016 (Fig. 1), of whom 29 are female. Inclusion criteria were age 40–80, complaints of cognitive decline relative to the previously normal state and Scandinavian first language. Exclusion criteria were established dementia, previous brain injury (including recognized stroke), neurodevelopmental disorder, and established serious psychiatric or somatic disorder, as well as drug use (including chemotherapy), which could significantly influence the cognitive function. All enrolled subjects had a standardized clinical assessment including physical examination, magnetic resonance imaging (MRI), lumbar puncture

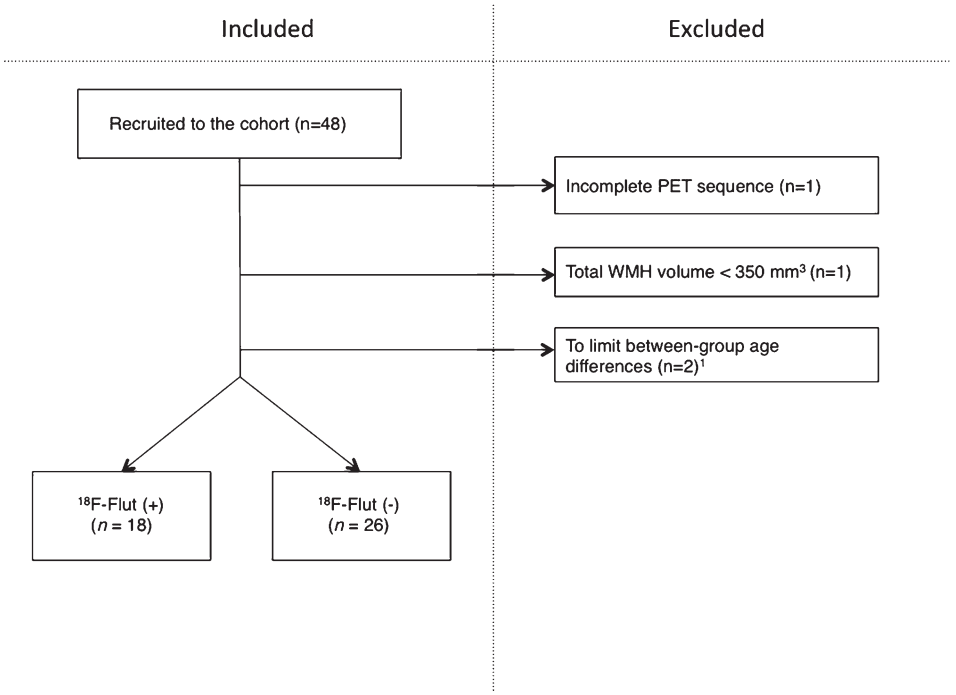

Fig. 1. Inclusions and exclusions in the cohort. Two subjects of <55 years of age were excluded to limit between-group age differences. PET, positron emission tomography; WMH, white matter hyperintensities; ^{18}F-Flut, ^{18}F-Flutemetamol.

($n = 42$), ^{18}F-Flut PET ($n = 48$), and ^{18}F-FDG PET ($n = 34$). All of the abovementioned procedures were performed within 3.5 months at the given assessment. The current data were collected either from time of inclusion (baseline) ($n = 28$), or at second assessment two years after inclusion ($n = 20$), given that they had not converted to dementia. The investigators were blinded to the subjects' identities.

Physicians trained in diagnosing cognitive disorders established the final diagnoses in consensus conferences. Almdahl et al. have described the diagnostic criteria, including the cognitive test battery, in detail [30]. Mild cognitive impairment (MCI, $n = 15$) was defined according to the core criteria in the recommendations from the National Institute on Aging/Alzheimer's Association (NIA/AA) [31]. Subjective cognitive decline (SCD) ($n = 29$) was defined based on the recommendations by the Subjective Cognitive Decline Initiative Working Group [32]. All forty-eight subjects had preserved functions of daily living, with Clinical Dementia Rating score ≤ 0.5 [33], i.e., not demented. Two subjects were classified as preclinical AD stage 2 according to recommendations from the NIA/AA [34], based on one positive amyloid marker (positive ^{18}F-Flut PET) and evidence of neuronal injury (pathological CSF total and/or phosphorylated tau). Two additional subjects were classified as preclinical AD stage 3 according the NIA/AA criteria, based on positive ^{18}F-Flut PET, evidence of neurodegeneration (pathological CSF tau), and with subtle cognitive decline.

One subject was excluded from the current study due to an incomplete PET scan (one frame only). One subject was excluded due to total WMH volume <350 mm^3, as we considered this as a minimum volume for robust analyses. Between-group age differences were limited by excluding subjects aged <50 years ($n = 2$). The remaining forty-four subjects were dichotomized according to cortical ^{18}F-Flut PET uptake and classified as positive (^{18}F-Flut(+)) or negative (^{18}F-Flut(–)), as determined by visual interpretation by trained readers blinded to any clinical information and CSF Aβ_{42}. The images were compared to a normal brain database supplied by the manufacturer of the tracer (CortexID, GE Healthcare, Chicago, IL, USA) and the subjects were classified as ^{18}F-Flut(+) or ^{18}F-Flut(–) according to the manufacturer's guidelines.

Written informed consent was obtained from all participants prior to enrollment. The study was approved by the Regional Committee for Medical

and Health Research Ethics, South East Norway (approval 2013/150) and conducted in accordance with the Helsinki Declaration.

MRI/PET Imaging acquisition

MRI was performed on a Philips Ingenia 3 Tesla system. A 3D T1-weighted turbo field echo sequence (TR/TE/TI/FA = 4.5 ms/2.2 ms/853 ms/8°, matrix = 256 × 213, 170 slices, thickness = 1.2 mm, in-plane resolution of 1 mm × 1.2 mm) and a 3D axial fluid-attenuated inversion recovery (FLAIR) sequence (TR/TE/TI = 8000 ms/418 ms/2400 ms, slice thickness = 1.2 mm) were obtained.

^{18}F-Flut and ^{18}F-FDG PET were obtained from the same GE Discovery 690 PET/CT scanner on two separate days. Subjects fasted at least 6 hours in advance and blood glucose was routinely measured prior to ^{18}F-FDG injection (subjects did not continue if blood glucose exceeded 8.0 mmol/l). For both the ^{18}F-FDG and ^{18}F-Flut scan sessions, a bolus injection of 185 MBq (5 mCi) was followed by rest before positioning the subject head-first supine in the scanner. Prior to PET acquisition, a low-dose CT scan for attenuation correction was acquired. PET scanning in 3D-mode started 45 minutes after injection of ^{18}F-FDG and 90 minutes after ^{18}F-Flut. PET data were acquired for 10 minutes for ^{18}F-FDG (six frames) and for 20 minutes (four frames of five minutes) for ^{18}F-Flut. Acquired data were corrected for random events, dead time, attenuation, scatter, and decay. PET volumes were reconstructed using an iterative algorithm (VUE Point FX SharpIR with six iterations, 24 subsets for ^{18}F-FDG, four iterations, 16 subsets for ^{18}F-Flut) and a post-reconstruction 3D Gaussian filter of 3 mm full-width half maximum was applied. The PET detector was cylindrical, 700 mm in the xy-plane and 153 mm in the z-plane, and there were 47 slices for both ^{18}F-FDG and ^{18}F-Flut. The matrix was 256 × 256 for ^{18}F-FDG and 192 × 192 for ^{18}F-Flut. Slice thickness was thus 3.27 mm for both ^{18}F-FDG and ^{18}F-Flut, original (xy plane) pixel size 3.27 mm × 3.27 mm for ^{18}F-FDG and 3.64 mm × 3.64 mm for ^{18}F-Flut.

Image processing

For the quantitative assessment, motion correction of the ^{18}F-Flut PET was performed using frame-by-frame rigid registration, then the frames were summed to a single time-frame image and rigidly registered to the anatomical MRI volume using a 6-parameter rigid registration as implemented in the Spatial Parametrical Mapping (SPM 12, Wellcome Trust Centre for Neuroimaging, UCL, UK) toolbox.

Due to the relatively poor scanner resolution, PET images are susceptible to partial volume effects. Because these spill-over effects may impact the quantification of the regional uptake [15], we recently developed an algorithm to correct for partial volume effects [35]. This is a voxel-based algorithm that relies on MRI based segmentation of anatomical regions and accurate measurements of the effective point spread function of the PET imaging process. The PVC algorithm was applied to the ^{18}F-Flut- and ^{18}F-FDG PET images using an estimated PSF of 5.34 × 4.79 × 5.55 mm [36]. ^{18}F-Flut- and ^{18}F-FDG PET images and structural images were further co-registered to high-resolution 3D T1-weighted MRI scans for WMH segmentation and measurements. Registrations were manually inspected for accuracy.

An in-house developed object-based supervised machine-learning algorithm was used for automated segmentation and quantification of WMHs based on FLAIR image intensity and masks of tissue types [37]. For all segmentations, a single investigator (LFK) performed manual inspection of accuracy and edited when necessary. The reconstruction and segmentation of WM was performed with the FreeSurfer image analysis suite version 5.3.0 (http://surfer.nmr.mgh.harvard.edu/). This includes segmentation of the subcortical white-matter and deep grey-matter volumetric structures, and parcellation of the cortical surface. NAWM was defined by subtracting WMH from the total WM. Analyses and calculations were performed using The Oxford Centre for Functional MRI of the Brain (FMRIB) Software Library (FSL) version 5.0 [38, 39]. ^{18}F-Flut and ^{18}F-FDG standardized uptake value ratios (SUVr) were obtained by normalization to the cerebellar cortex. Prior to normalization, the cerebellar mask was eroded by 1 mm to avoid partial volume effects, inaccurate segmentation or co-registration. ^{18}F-Flut and ^{18}F-FDG uptake were analyzed in five pre-selected cortical regions of interest (ROIs), as defined by Desikan et al. [40], known to hold substantial amyloid plaques in AD: the precuneus and posterior cingulate combined, anterior cingulate, prefrontal, inferior parietal, and lateral temporal cortex [41]. These are also the regions used for clinical evaluation of ^{18}F-Flut status according to the manufacturer's guidelines [42]. We chose to only include early predilection sites for amyloid deposition in this subanalysis. We further calculated a

composite SUVr by averaging the uptake in the above-mentioned regions. For comparative purposes, the ^{18}F-Flut uptake was also analyzed in the hippocampus, parahippocampal gyrus, and entorhinal cortex. The ^{18}F-Flut and ^{18}F-FDG uptake for each region were averaged across the hemispheres, and the cerebellar cortex was used as the reference region.

Cerebrospinal fluid analyses

Lumbar puncture was performed consecutively after inclusion, between 8 a.m. and noon, at the L3/L4, L4/L5, or L5/S1 interspace. CSF was examined for the traditional CSF biomarkers Aβ_{42}, T-tau, and P-tau and quantified with commercially available ELISAs (Fujirebio Europe, Gent, Belgium). The analyses were carried out in accordance with the manufacturers' instructions at the national reference laboratory for these tests at the Department of Interdisciplinary Laboratory Medicine and Medical Biochemistry, Akershus University Hospital. The laboratory recommends the following cut-off values for abnormality (modified from Sjögren et al. [43]); t-tau >300 pg/ml for age <50 years, >450 pg/ml for age 50–69 years, and >500 pg/ml for age ≥70 years, p-tau ≥ 80 pg/ml and Aβ_{42} < 550 pg/ml. The national reference laboratory is part of the European multicenter project "Biomarkers for Alzheimer's disease and Parkinson's disease" (BIOMARKAPD), funded by EU Joint Programme-Neurodegenerative Disease Research (JPND), for standardization of analytical methods and laboratory procedures to increase its accuracy with regard to CSF biomarkers of neurodegenerative diseases.

Statistical analyses

Demographic and clinical features were assessed using chi-square tests for categorical data and independent-samples *T*-test or Mann-Whitney U test for continuous data. The WMH volume was logarithmically transformed prior to group-difference analyses.

Regional cortical ^{18}F-Flut and CSF Aβ_{42}

To determine the CSF Aβ_{42} concentrations associated with abnormal ^{18}F-Flut uptake, slope and intercept values from regression equations representing associations between regional ^{18}F-Flut and CSF Aβ_{42} were used. Abnormal ^{18}F-Flut SUVr was defined as SUVr > 1.46, as previously published [44]. Receiver operating characteristic (ROC) curves were used to determine the sensitivity and specificity of the different CSF Aβ_{42} concentrations (as compared to ^{18}F-Flut). All SUVr were PVE corrected. Linear regression was used to correct for age and sex, and the residuals were used for correlation analyses.

Associations between cortical ^{18}F-Flut and ^{18}F-FDG uptake

Spearman correlations were computed for assessment of associations between regional ^{18}F-Flut SUVr and CSF Aβ_{42}, as well as correlations between cortical ^{18}F-Flut and ^{18}F-FDG SUVr. All SUVr were PVE corrected.

Regional ^{18}F-Flutemetamol retention and relevance to white matter pathology

We investigated ^{18}F-Flut uptake prior to normalization to reference regions, exploring a putative pathology-specific increased retention in regions commonly used as reference for intensity normalization. Such standardized uptake values (SUV) were also analyzed in cerebral WM, WMHs, and NAWM for comparative purposes. SUV was calculated by dividing the mean regional radioactivity by the injected dose and body weight. SUVr were analyzed for cortical regions. Hippocampal, parahippocampal and entorhinal SUVr were analyzed for comparative purposes. Ratios were calculated by dividing the uptake for each region in ^{18}F-Flut(+) by ^{18}F-Flut(–), and Independent Samples *T*-tests and Mann-Whitney *U* tests were conducted to test for significance. For SUVr age and total WMH volume were included as covariates.

To analyze the potential use of ^{18}F-Flut as a marker of WM pathology, ^{18}F-Flut uptake in WMH and NAWM were determined prior to and after normalization to reference region, and group differences (i.e., ^{18}F-Flut(+) versus ^{18}F-Flut(–)) were assessed with Independent-Samples *T*-Tests. ^{18}F-Flut WMHs retention was logarithmically transformed prior to the analyses. Age and total WMH volume were included as covariates for analyses of SUVr, and the ensuing residuals were normally distributed. Retention in WMHs and NAWM were compared using Paired-Samples *T* test. For assessment of the WMHs binding of ^{18}F-Flut, we investigated associations between the ^{18}F-FDG SUVr and ^{18}F-Flut SUVr in WMHs using Spearman correlation. Linear regression was used to correct for age and total WMH volume, and the resulting residuals were used for the correlation analyses. In addition, Spearman correlations

were used to determine associations between ^{18}F-Flut SUVr in WMHs and cortex, as well as associations between ^{18}F-FDG SUVr in WMHs and cortical ^{18}F-Flut SUVr.

All tests were performed with significance level set at $p < 0.05$. Statistical analyses were performed with SPSS version 23 (SPSS Inc., Chicago, IL, USA).

RESULTS

Demographic and clinical data are listed in Table 1. There were no significant group differences in sex, age, WMH volume, or Mini-Mental State Examination score. By design, ^{18}F-Flut (+) presented with significantly lower CSF Aβ_{42} and larger cortical SUVr of ^{18}F-Flut when compared to ^{18}F-Flut (–).

Regional cortical ^{18}F-Flut and CSF Aβ_{42}

We compared regional cortical SUVr of ^{18}F-Flut and CSF Aβ_{42}. Figure 2 summarizes the results, and illustrates the CSF Aβ_{42} concentration (vertical dotted line) at which abnormal ^{18}F-Flut SUVr (>1.46, horizontal dotted line) would be identified for each AD-specific region (also the composite region). Corresponding CSF Aβ_{42} levels ranged from 645 pg/ml in the anterior cingulate cortex to 762 pg/ml in the inferior parietal lobe, yielding sensitivities 87–93% and specificities 85–93% (Fig. 3). There were strong negative correlations between CSF Aβ_{42} and ^{18}F-Flut SUVr for all regions; precuneus and posterior cingulate cortex ($r = –0.85$, $p < 0.001$), anterior cingulate cortex ($r = –0.76$, $p < 0.001$), prefrontal lobe ($r = –0.68$, $p < 0.001$), inferior parietal lobe ($r = –0.79$, $p < 0.001$) and lateral temporal lobe ($r = –0.72$, $p < 0.001$).

Associations between cortical ^{18}F-Flut and ^{18}F-FDG uptake

There were strong negative Spearman correlations between regional cortical ^{18}F-Flut and ^{18}F-FDG uptake in ^{18}F-Flut(+) subjects in the precuneus and posterior cingulate ($r = –0.797$, $p = 0.002$), anterior cingulate cortex ($r = –0.699$, $p = 0.011$), inferior parietal lobe ($r = –0.727$, $p = 0.007$), lateral temporal lobe ($r = –0.622$, $p = 0.031$), as well as the prefrontal lobe ($r = –0.811$, $p = 0.001$). No significant correlations were observed in ^{18}F-Flut(–) subjects.

Regional ^{18}F-Flutemetamol retention and relevance to white matter pathology

^{18}F-Flut SUVs (i.e., prior to intensity normalization against a reference region) were analyzed in several regions, in both PVE corrected and uncorrected images, primarily to investigate the validity of typical reference regions used for further analyses. We found numerically higher retention in all regions in subjects classified as ^{18}F-Flut(+) compared to ^{18}F-Flut(–). Based on the comparison of the SUV values between possible reference regions, we used the cerebellum cortex as reference region to calculate SUVr values. Before PVE correction, significant differences were also observed in subcortical WM and NAWM. Cortical ROIs were analyzed using SUVr. As expected, highly significant differences were observed in cortical regions ($p < 0.001$) when comparing ^{18}F-Flut(+) and ^{18}F-Flut(–). Results are summarized in Table 2.

White matter hyperintensities. Before and after PVE corrections ^{18}F-Flut SUVs were higher in WMHs in ^{18}F-Flut(+) compared to ^{18}F-Flut(–) (Table 2). No significant difference ($p = 0.112$) was observed in NAWM when comparing ^{18}F-

Table 1
Characteristics of the cohort

	Total study cohort ($n = 44$)	^{18}F-Flut (+) ($n = 18$)	^{18}F-Flut (–) ($n = 26$)	p-value (^{18}F-Flut(+) versus ^{18}F-Flut(–))
Age, y	65.91 (6.88)	68.17 (4.80)	64.35 (7.72)	0.070[a]
Women, n (%)	25 (56.8)	10 (55.56)	15 (57.69)	0.890[b]
MMSE, points	28.53 (1.52)	28.06 (1.89)	28.85 (1.16)	0.208[c]
CSF Aβ_{42} (pg/ml)	873.57 (320.04)	567.19 (167.31)	1062.12 (232.67)	**<0.001[a]**
WMH volume (mm^3)	5850.50 (7235.81)	7280.00 (9372.94)	4860.85 (5274.92)	0.448[a,d]

Values are given in mean (standard deviation). Statistically significant differences shown in bold. [a]Independent-samples T-test. [b]Pearson Chi-square test. [c]Mann-Whitney U test. [d]p-value for log transformed WMH volume adjusted for age. ^{18}F-Flut, ^{18}F-Flutemetamol; MMSE, Mini-Mental State Examination; CSF, cerebrospinal fluid; Aβ, amyloid β-peptide; WMH, white matter hyperintensities.

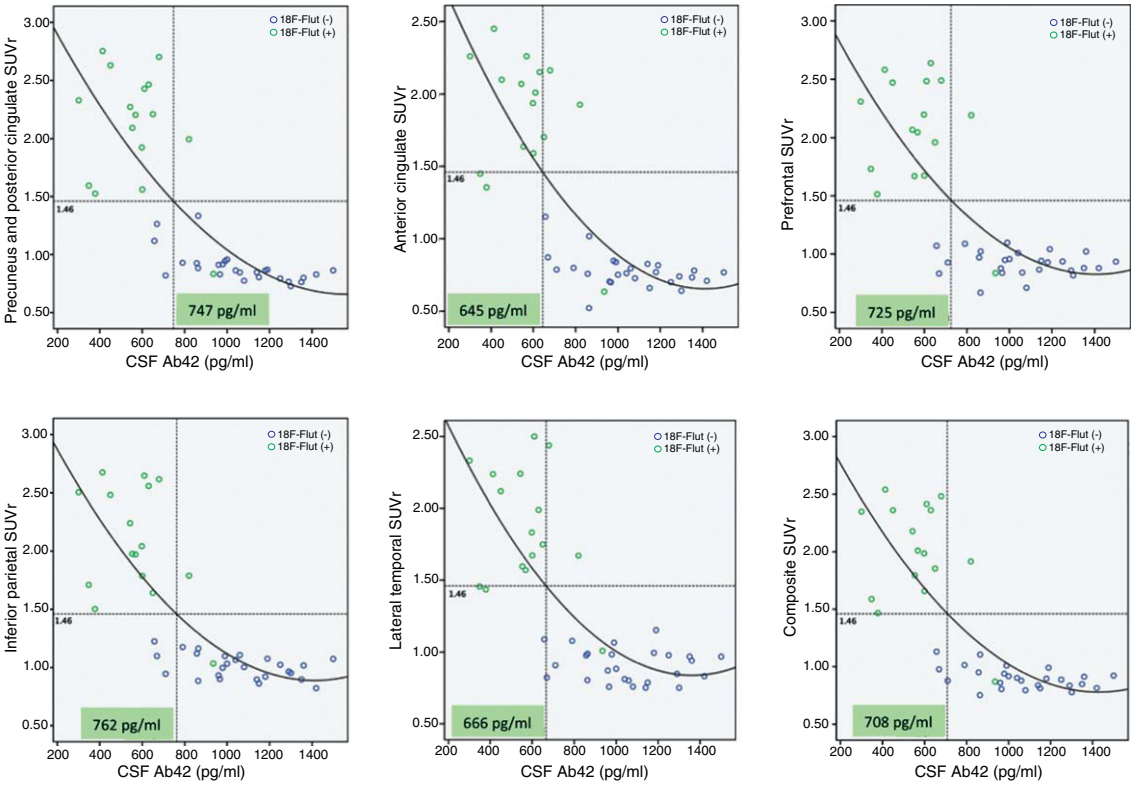

Fig. 2. Associations between regional ^{18}F-Flutemetamol SUVr and CSF Aβ_{42}. Based on the visual interpretation by a trained reader, the subjects are marked as ^{18}F-Flut(+) (green dots) or ^{18}F-Flut(–) (blue dots). Using an SUVr cut-off of 1.46 yields different CSF Aβ_{42} cut-offs for each pre-selected region. SUVr, standardized uptake value ratios; CSF, cerebrospinal fluid; Aβ_{42}, amyloid-β 1-42.

Table 2
Regional ^{18}F-Flutemetamol uptake in ^{18}F-Flut(+) versus ^{18}F-Flut(–)

	PVE corrected				PVE uncorrected			
	^{18}F-Flut +	^{18}F-Flut–	Ratio	*p*	^{18}F-Flut +	^{18}F-Flut –	Ratio	*p*
A. SUV								
WMH	767.72 (193.92)	633.21 (173.71)	1.21	**0.015**[a]	700.66 (170.81)	575.13 (159.05)	1.22	**0.019**[a]
NAWM	1028.62 (190.89)	932.33 (240.24)	1.10	0.112[a]	978.49 (187.30)	848.64 (224.09)	1.15	**0.035**[a]
WM	1020.95 (195.67)	913.18 (242.43)	1.12	0.081[a]	918.69 (187.59)	749.75 (211.26)	1.23	**0.007**[a]
Cerebellum cortex	429.59 (109.05)	389.58 (142.53)	1.10	0.143[a]	429.13 (112.64)	391.34 (147.88)	1.10	0.169[a]
Cerebellum WM	921.76 (192.45)	830.06 (248.26)	1.11	0.121[a]	920.51 (192.29)	828.68 (248.16)	1.11	0.120[a]
Brainstem	1025.93 (233.15)	933.80 (305.42)	1.10	0.157[a]	1031.65 (232.99)	938.33 (307.75)	1.10	0.157[a]
B. SUVr								
Precun + post.cing.	2.17 (0.54)	0.89 (0.14)	2.44	**<0.001**[b]	1.97 (0.31)	1.23 (0.14)	1.60	**<0.001**[b]
Anterior cingulate	1.94 (0.50)	0.78 (0.12)	2.49	**<0.001**[b]	1.88 (0.28)	1.20 (0.13)	1.57	**<0.001**[b]
Prefrontal	2.15 (0.53)	0.92 (0.11)	2.34	**<0.001**[b]	1.78 (0.28)	1.13 (0.10)	1.58	**<0.001**[b]
Inferior parietal	2.15 (0.50)	1.01 (0.11)	2.13	**<0.001**[b]	1.80 (0.27)	1.21 (0.11)	1.49	**<0.001**[b]
Lateral temporal	1.92 (0.43)	0.91 (0.12)	2.11	**<0.001**[b]	1.70 (0.23)	1.17 (0.10)	1.45	**<0.001**[b]
Hippocampus	1.07 (0.07)	1.05 (0.06)	1.02	0.274[b]	1.25 (0.10)	1.24 (0.12)	1.01	0.526[b]
Parahippocampal	1.33 (0.26)	0.76 (0.09)	1.75	**<0.001**[b]	1.35 (0.12)	1.07 (0.10)	1.26	**<0.001**[b]
Entorhinal	1.14 (0.24)	0.90 (0.09)	1.27	**0.002**[b]	1.19 (0.14)	1.04 (0.12)	1.14	**0.003**[b]

Values are given in standardized uptake value (SUV) in A and in standardized uptake value ratio (SUVr) in B. [a]Calculated using Independent-samples *T* test. [b]Calculated using Mann-Whitney *U* test. Ratio and *p*-values indicate ^{18}F-Flut + versus ^{18}F-Flut –. Statistically significant group differences are shown in bold. PVE, partial volume effects; WMH, white matter hyperintensities; NAWM, normal-appearing white matter; WM, white matter.

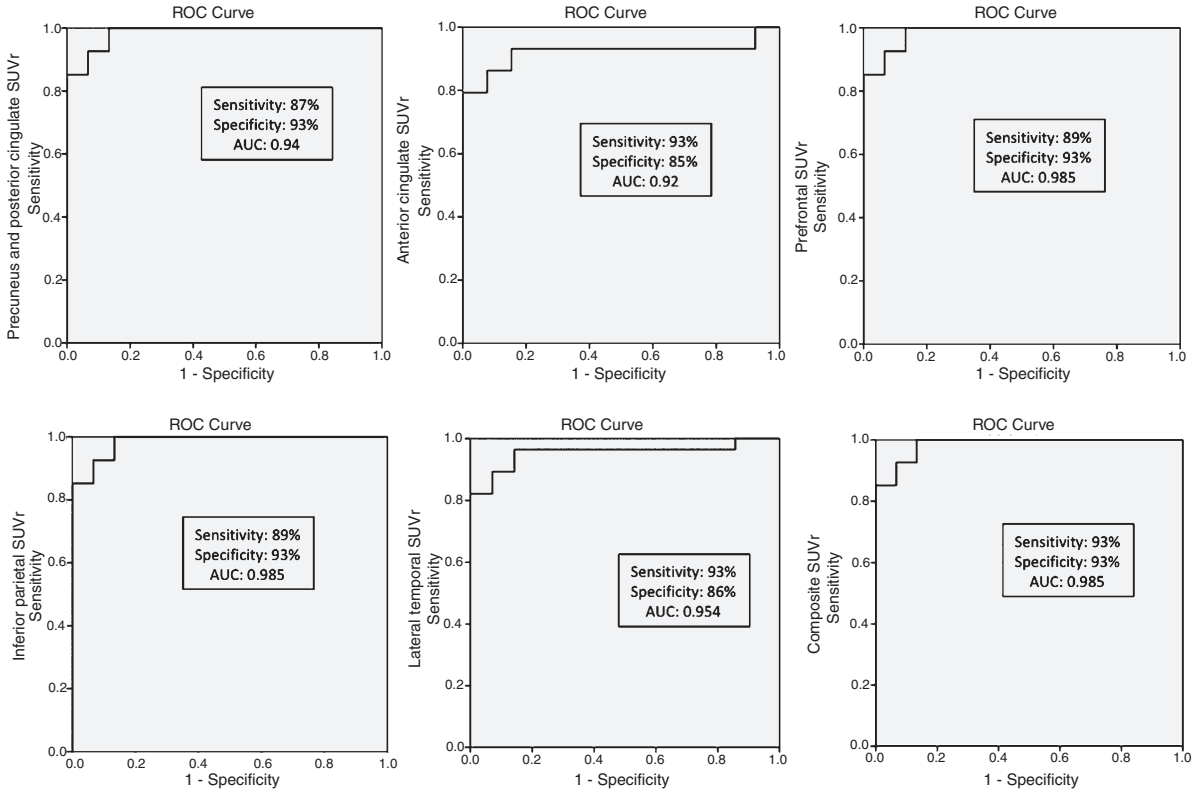

Fig. 3. Receiver operating characteristic (ROC) curves for the accuracy of each CSF $A\beta_{42}$ cut-off to predict regional ^{18}F-Flutemetamol abnormality.

Flut(+) (mean = 1028.62, SD = 190.89) and ^{18}F-Flut(–) (mean = 932.33, SD = 240.24). When normalizing against a reference region, corrected for age and total WMH volume, the group differences in WMHs were considerably reduced ($p = 0.414$; ^{18}F-Flut(+) mean SUVr = 1.82, SD = 0.34; ^{18}F-Flut(–) mean SUVr = 1.69, SD = 0.25) and not significant. No significance was observed in NAWM ($p = 0.218$; ^{18}F-Flut(+) mean SUVr = 2.44, SD = 0.30; ^{18}F-Flut(–) mean SUVr = 2.50, SD = 0.39). We found significantly reduced retention in WMHs compared to NAWM ($Z = –5{,}78$, $p < 0{,}001$), presenting with a reduction of 29.81%. We further assessed correlations between the ^{18}F-Flut SUVr and ^{18}F-FDG SUVr in WMHs and found strong positive correlations in ^{18}F-Flut(+) subjects ($r = 0.779$, $p = 0.003$), while no significant correlation was found in ^{18}F-Flut(–) subjects ($r = 0.200$, $p = 0.371$).

Associations between ^{18}F-Flut SUVr in WMHs and GM, and between ^{18}F-FDG SUVr in WMHs and cortical ^{18}F-Flut SUVr were assessed (Table 3). ^{18}F-FDG uptake in WMHs and cortical ^{18}F-Flut SUVr in the AD-predilection cortical regions were negatively correlated. No significant correlations were found between ^{18}F-Flut uptake in WMHs and cortex.

DISCUSSION

In this study, we combined three AD biomarkers, CSF $A\beta_{42}$, ^{18}F-Flut - and ^{18}F-FDG PET, finding that CSF $A\beta_{42}$ concentrations associated with abnormal ^{18}F-Flut uptake differ between predilection areas for AD pathology, posterior areas demonstrating a pathological high retention at higher CSF $A\beta_{42}$ levels. . We showed strong negative correlations between cortical ^{18}F-Flut and ^{18}F-FDG uptake. To our knowledge, we are the first to evaluate the use of ^{18}F-Flut in WMHs. We found generally higher ^{18}F-Flut retention throughout the brain in ^{18}F-Flut(+) subjects prior to normalization, including subcortical WM. We found significantly higher WMH ^{18}F-Flut uptake in ^{18}F-Flut(+) as compared to ^{18}F-Flut(–) without normalizing to a reference region, but after normalization the differences were noticeably reduced.

Table 3
Associations between ^{18}F-Flutemetamol and ^{18}F-FDG SUVr in WMHs and cortical ^{18}F-Flutemetamol

	^{18}F-Flutemetamol in WMHs	^{18}F-FDG in WMHs
^{18}F-Flutemetamol in		
Precuneus + post.cing	$r = 0.068$, $p = 0.663$	**$r = -0.359$, $p = 0.037$**
Anterior cingulate	$r = 0.046$, $p = 0.786$	**$r = -0.469$, $p = 0.005$**
Prefrontal	$r = -0.018$, $p = 0.908$	**$r = -0.396$, $p = 0.020$**
Inferior parietal	$r = 0.004$, $p = 0.978$	**$r = -0.422$, $p = 0.013$**
Lateral temporal	$r = -0.064$, $p = 0.681$	**$r = -0.358$, $p = 0.037$**
Hippocampus	$r = 0.009$, $p = 0.952$	$r = 0.077$, $p = 0.666$
Parahippocampus	$r = 0.139$, $p = 0.367$	$r = -0.246$, $p = 0.161$
Entorhinal cortex	$r = 0.086$, $p = 0.579$	$r = -0.267$, $p = 0.127$

Significance shown in bold. SUVr, standardized uptake value ratios; FDG, fluorodeoxyglucose; WMHs, white matter hyperintensities.

Brain amyloid pathology is a core diagnostic clinical criterion of AD, as evidenced by low CSF Aβ_{42} or positive amyloid PET. CSF biomarkers have shown similar diagnostic accuracy as both regional and composite PET measures [5]. CSF was recently demonstrated to reliably predict Aβ accumulation, where a CSF Aβ_{42} concentration of 647 pg/ml or less identified a positive composite ^{18}F-Flut PET measure with high sensitivity and specificity [4]. However, regional differences in this aspect have not been investigated. In the current study, we find that regions known to harbor amyloid plaques in AD show abnormal ^{18}F-Flut retention at different CSF Aβ_{42} concentrations (the inferior parietal lobe and posterior cingulate and precuneus present with abnormal ^{18}F-Flut SUVr at the highest concentrations, followed by the prefrontal cortex). There were strong negative correlations between CSF Aβ_{42} and ^{18}F-Flut SUVr in these regions, in line with previous findings [4], and our analyses yielded sensitivity and specificity around 90% for all investigated regions and CSF cut-offs (Fig. 3). The current findings are supported by the early involvement of these regions in the disease course [41] and local predilection for plaque deposition [45].

This gives additional valuable information for CSF as a clinical tool, also considering the ^{18}F-Flut manufacturer's guidelines stating that a positive ^{18}F-Flut PET scan requires abnormal amyloid retention in at least one region [42]. This highlights the need for standardization of CSF biomarker analyses to define the optimal threshold for abnormal values. There is generally a large span in the CSF Aβ_{42} cut-offs and cut-offs reported in the current study are slightly higher than what Palmqvist et al. found [4]. This may result from the known between-laboratory variability in CSF Aβ_{42} analyses. There is a need for validation of these cut-offs to increase the diagnostic accuracy of CSF biomarkers, as CSF is an amenable clinical tool in many circumstances, and also to reduce the chances of false negatives.

Reduced cerebral glucose metabolism, as determined by ^{18}F-FDG PET, is a well-established feature of AD [46]. Previous studies combining amyloid PET and ^{18}F-FDG PET report conflicting results, some showing reduced glucose metabolism with increasing Aβ load [47, 48], while others do not [49, 50]. When associations were observed, they seemed to be region-specific, involving mostly posterior brain regions. This is consistent with our findings of significant cortical regional correlations, with the strongest correlations observed in the precuneus, posterior cingulate and inferior parietal lobe, and additional prefrontal regions. These predilection sites mimic early changes in ^{18}F-Flut versus CSF (as described above). Significant associations were only found in ^{18}F-Flut(+) subjects, which may not be surprising due to the by design low cortical uptake in ^{18}F-Flut(–) subjects. However, it may also support previous hypotheses of toxic effects of Aβ on synaptic function in AD [47], as increased fibrillar Aβ (as is detected with amyloid PET) has been associated with higher levels of toxic oligomers [51].

We further investigated regional ^{18}F-Flut retention (Table 2). As expected, significantly higher cortical uptake was observed in ^{18}F-Flut(+) compared to ^{18}F-Flut(–), using SUVr (Table 2 B). PET images are prone to PVE [52], primarily due to low spatial resolution, resulting in biased uptake measurements due to spill-over. For amyloid PET there may be an overestimation of cortical retention in healthy controls more than in AD due to relatively high WM retention, increasing the chances for false positives [53]. Therefore, correcting for PVE may improve statistical power [15]. This is illustrated by the higher cortical uptake in PVE uncorrected images compared

to corrected images in ^{18}F-Flut(–) subjects, likely due to spill-over from WM. Similarly, in ^{18}F-Flut(+) subjects there may be a spill-over from GM to subcortical WM, illustrated by slightly larger ratios in PVE uncorrected compared to corrected images, causing a positive bias and overestimation of WM signal. This highlights the importance of such a correction, not only for accurate quantification of the cortical signal, but also for potential WM analyses.

SUV was used to investigate the validity of typical reference regions, for further analyses of WM (Table 2A). This was done because group differences in reference regions may potentially impact SUVr, especially in regions with more subtle differences in ^{18}F-Flut uptake, e.g., WM. Higher SUV in ^{18}F-Flut(+) was also observed in subcortical WM, with significant difference in WMHs, with and without PVE correction. Analyses with and without PVE correction were performed to investigate the potential impact of such correction also in WM analyses, as it is shown to increase the accuracy of analyses [15]. The high WM retention reported with ^{18}F-Flut raises the possibility of ^{18}F-Flut being a marker for WM pathology, though the binding characteristics of ^{18}F-Flut in WM remain to be determined. We investigated subcortical retention in ^{18}F-Flut(+) and ^{18}F-Flut(–) to further explore the possible relationship between amyloid and WM pathology as this may improve the understanding of associations between CVD and AD. Investigating ^{18}F-Flut retention in WMHs, we found significant group differences in WMH ^{18}F-Flut uptake when comparing SUVs (i.e., prior to normalization) in ^{18}F-Flut(+) and ^{18}F-Flut(–), with the highest retention in ^{18}F-Flut(+). The differences were noticeably reduced when normalizing the uptake to a reference region (SUVr) and no longer significant. There is generally a slightly higher ^{18}F-Flut retention in subjects classified as ^{18}F-Flut(+), and a possible explanation for the reduction in differences may be the observed higher aberrant uptake across the entire brain in ^{18}F-Flut(+) subjects, including the typical reference regions cerebellum and brainstem in which specific binding is believed to be negligible. Furthermore, the findings must be interpreted with caution, as several factors are known to impact on SUV, and SUVr is considered the more precise and robust measure for amyloid PET.

High WM retention has been reported for several ^{18}F-PET ligands [10, 54, 55]. The WM binding of ^{18}F-Flut was recently investigated using spectral analysis and the authors concluded that WM binding was nonspecific, i.e., not related to amyloid binding [13]. This is in line with what has previously been reported with ^{18}F-Florbetaben using kinetic model-based analyses [55]. This is supported by the current associations observed between ^{18}F-Flut and ^{18}F-FDG uptake in WMHs, as well as the lack of correlations between the ^{18}F-Flut uptake in WMHs and cortex in the current study. Accumulating evidence links CVD and AD [19], and we have previously demonstrated impaired WMH microstructural integrity in Aβ positive subjects using diffusion tensor imaging [17]. Furthermore, we recently found reduced glucose metabolism in WMHs in the presence of amyloid dysmetabolism [16]. Increased fibrillar Aβ has been associated with higher levels of Aβ oligomers, suggested to be more neurotoxic and promote neurodegeneration [56]. Hence, the current findings of negative associations between the ^{18}F-FDG uptake in WMHs and cortical ^{18}F-Flut retention support our previous findings [16], connecting increasing Aβ pathology to glucose hypometabolism in WMHs.

Tracer tissue extraction and clearance is related to cerebral blood flow (CBF), and CBF decreases during AD progression [22]. WMHs are often considered to result from hypoperfusion [57], and previous studies using ^{11}C-PiB found reduced retention in WMHs compared to NAWM [25–27]. This has in addition been reported with another ^{18}F-PET ligand, ^{18}F-Florbetaben [58], and we observed the same with ^{18}F-Flut in the current study. Hence one might expect lower ^{18}F-Flut uptake in WMHs in ^{18}F-Flut(+). However, SUVr do not distinguish between the contributions of CBF and clearance, and clearance also depends on the capillary integrity, known to be reduced in AD [22]. In CAA type 1, as opposed to CAA type 2 (involving larger vessels), the capillaries are affected, reflected by Aβ deposition in the outer basement membrane [24]. Similar to Aβ plaques, these vascular changes present with surrounding microglia activation and inflammatory responses [59]. The vascular bed in AD further presents with several alterations. The microvascular distortion and capillary dysfunction affects the neurovascular unit, thereby affecting the blood-brain barrier function [60] causing impaired clearance of soluble substances [22, 23]. Given little or absent specific ^{18}F-Flut amyloid binding in WM, one possible explanation for the higher ^{18}F-Flut retention observed in WMHs in ^{18}F-Flut(+) subjects might be vascular damage present in AD impairing tracer clearance. The lack of difference observed in NAWM raises the possibility that these alterations are confined to WMHs. For other ^{18}F-ligands, white matter retention

has also been hypothesized to result from reduced WM blood perfusion compared to the cortex and thus slower clearance [61]. However, due to the aberrant uptake observed ^{18}F-Flut (+), we cannot conclude that ^{18}F-Flut is a suitable marker for WM pathology and the current findings must be interpreted with caution. Replications in larger cohorts are warranted for further assessment of the use of ^{18}F-Flut in WM pathology.

The cross-sectional study design may be a limitation when considering regional comparisons of cortical ^{18}F-Flut retention and CSF Aβ_{42} in patients destined to develop dementia due to AD, and longitudinal studies should be conducted for further evaluations of the regional Aβ depositions related to CSF Aβ_{42} cut-offs.

In conclusion, although the study design and the relatively small sample size are limitations and replications in larger cohorts are warranted, this study gives further evidence for CSF Aβ_{42} as a clinical tool to predict regional cortical Aβ deposition. In addition, our findings support previous hypotheses of toxic effects of Aβ on synaptic function based on the strong correlations observed between cortical ^{18}F-Flut and ^{18}F-FDG uptake. Furthermore, we replicate our previous findings [16] linking amyloid dysmetabolism to glucose hypometabolism in WMHs. We also demonstrate generally higher ^{18}F-Flut retention across the brain in subjects classified as ^{18}F-Flut(+), including WM and WMHs, which may challenge the use of ^{18}F-Flut for WM analyses. Hence replications in larger cohorts are warranted for further assessment of the use of ^{18}F-Flut in WM pathology.

ACKNOWLEDGMENTS

Study funded by The Research Council of Norway (grant reference number 217780/H10); South-Eastern Norway Regional Health Authority (grant reference number 2013131); and EU-JPND via The Research Council of Norway (grant reference number 237250).

Authors' disclosures available online (https://www.j-alz.com/manuscript-disclosures/17-0582r2).

REFERENCES

[1] Braak H, Braak E (1991) Neuropathological stageing of Alzheimer-related changes. *Acta Neuropathol* **82**, 239-259.

[2] Blennow K, Mattsson N, Scholl M, Hansson O, Zetterberg H (2015) Amyloid biomarkers in Alzheimer's disease. *Trends Pharmacol Sci* **36**, 297-309.

[3] Weigand SD, Vemuri P, Wiste HJ, Senjem ML, Pankratz VS, Aisen PS, Weiner MW, Petersen RC, Shaw LM, Trojanowski JQ, Knopman DS, Jack CR Jr. (2011) Transforming cerebrospinal fluid Abeta42 measures into calculated Pittsburgh Compound B units of brain Abeta amyloid. *Alzheimers Dement* **7**, 133-141.

[4] Palmqvist S, Zetterberg H, Blennow K, Vestberg S, Andreasson U, Brooks DJ, Owenius R, Hagerstrom D, Wollmer P, Minthon L, Hansson O (2014) Accuracy of brain amyloid detection in clinical practice using cerebrospinal fluid beta-amyloid 42: A cross-validation study against amyloid positron emission tomography. *JAMA Neurol* **71**, 1282-1289.

[5] Palmqvist S, Zetterberg H, Mattsson N, Johansson P, Minthon L, Blennow K, Olsson M, Hansson O (2015) Detailed comparison of amyloid PET and CSF biomarkers for identifying early Alzheimer disease. *Neurology* **85**, 1240-1249.

[6] Landau SM, Lu M, Joshi AD, Pontecorvo M, Mintun MA, Trojanowski JQ, Shaw LM, Jagust WJ (2013) Comparing positron emission tomography imaging and cerebrospinal fluid measurements of beta-amyloid. *Ann Neurol* **74**, 826-836.

[7] Cairns NJ, Ikonomovic MD, Benzinger T, Storandt M, Fagan AM, Shah AR, Reinwald LT, Carter D, Felton A, Holtzman DM, Mintun MA, Klunk WE, Morris JC (2009) Absence of Pittsburgh compound B detection of cerebral amyloid beta in a patient with clinical, cognitive, and cerebrospinal fluid markers of Alzheimer disease: A case report. *Arch Neurol* **66**, 1557-1562.

[8] Mattsson N, Zetterberg H, Hansson O, Andreasen N, Parnetti L, Jonsson M, Herukka SK, van der Flier WM, Blankenstein MA, Ewers M, Rich K, Kaiser E, Verbeek M, Tsolaki M, Mulugeta E, Rosen E, Aarsland D, Visser PJ, Schroder J, Marcusson J, de Leon M, Hampel H, Scheltens P, Pirttila T, Wallin A, Jonhagen ME, Minthon L, Winblad B, Blennow K (2009) CSF biomarkers and incipient Alzheimer disease in patients with mild cognitive impairment. *JAMA* **302**, 385-393.

[9] Klunk WE, Engler H, Nordberg A, Wang Y, Blomqvist G, Holt DP, Bergstrom M, Savitcheva I, Huang GF, Estrada S, Ausen B, Debnath ML, Barletta J, Price JC, Sandell J, Lopresti BJ, Wall A, Koivisto P, Antoni G, Mathis CA, Langstrom B (2004) Imaging brain amyloid in Alzheimer's disease with Pittsburgh Compound-B. *Ann Neurol* **55**, 306-319.

[10] Vandenberghe R, Van Laere K, Ivanoiu A, Salmon E, Bastin C, Triau E, Hasselbalch S, Law I, Andersen A, Korner A, Minthon L, Garraux G, Nelissen N, Bormans G, Buckley C, Owenius R, Thurfjell L, Farrar G, Brooks DJ (2010) 18F-flutemetamol amyloid imaging in Alzheimer disease and mild cognitive impairment: A phase 2 trial. *Ann Neurol* **68**, 319-329.

[11] Landau SM, Thomas BA, Thurfjell L, Schmidt M, Margolin R, Mintun M, Pontecorvo M, Baker SL, Jagust WJ (2014) Amyloid PET imaging in Alzheimer's disease: A comparison of three radiotracers. *Eur J Nucl Med Mol Imaging* **41**, 1398-1407.

[12] Kepe V, Moghbel MC, Langstrom B, Zaidi H, Vinters HV, Huang SC, Satyamurthy N, Doudet D, Mishani E, Cohen RM, Hoilund-Carlsen PF, Alavi A, Barrio JR (2013) Amyloid-beta positron emission tomography imaging probes: A critical review. *J Alzheimers Dis* **36**, 613-631.

[13] Heurling K, Buckley C, Vandenberghe R, Laere KV, Lubberink M (2015) Separation of beta-amyloid binding and

white matter uptake of (18)F-flutemetamol using spectral analysis. *Am J Nucl Med Mol Imaging* **5**, 515-526.

[14] Snellman A, Rokka J, Lopez-Picon FR, Eskola O, Wilson I, Farrar G, Scheinin M, Solin O, Rinne JO, Haaparanta-Solin M (2012) Pharmacokinetics of [(1)(8)F]flutemetamol in wild-type rodents and its binding to beta amyloid deposits in a mouse model of Alzheimer's disease. *Eur J Nucl Med Mol Imaging* **39**, 1784-1795.

[15] Thomas BA, Erlandsson K, Modat M, Thurfjell L, Vandenberghe R, Ourselin S, Hutton BF (2011) The importance of appropriate partial volume correction for PET quantification in Alzheimer's disease. *Eur J Nucl Med Mol Imaging* **38**, 1104-1119.

[16] Kalheim LF, Selnes P, Bjornerud A, Coello C, Vegge K, Fladby T (2016) Amyloid Dysmetabolism relates to reduced glucose uptake in white matter hyperintensities. *Front Neurol* **7**, 209.

[17] Kalheim LF, Bjornerud A, Fladby T, Vegge K, Selnes P (2017) White matter hyperintensity microstructure in amyloid dysmetabolism. *J Cereb Blood Flow Metab* **37**, 356-365.

[18] Wardlaw JM, Smith EE, Biessels GJ, Cordonnier C, Fazekas F, Frayne R, Lindley RI, O'Brien JT, Barkhof F, Benavente OR, Black SE, Brayne C, Breteler M, Chabriat H, Decarli C, de Leeuw FE, Doubal F, Duering M, Fox NC, Greenberg S, Hachinski V, Kilimann I, Mok V, Oostenbrugge R, Pantoni L, Speck O, Stephan BC, Teipel S, Viswanathan A, Werring D, Chen C, Smith C, van Buchem M, Norrving B, Gorelick PB, Dichgans M (2013) Neuroimaging standards for research into small vessel disease and its contribution to ageing and neurodegeneration. *Lancet Neurol* **12**, 822-838.

[19] Iadecola C (2013) The pathobiology of vascular dementia. *Neuron* **80**, 844-866.

[20] Selnes P, Grambaite R, Rincon M, Bjornerud A, Gjerstad L, Hessen E, Auning E, Johansen K, Almdahl IS, Due-Tonnessen P, Vegge K, Bjelke B, Fladby T (Metab) (2015) Hippocampal complex atrophy in poststroke and mild cognitive impairment. *J Cereb Blood Flow* **35**, 1729-1737.

[21] Ostergaard L, Jespersen SN, Mouridsen K, Mikkelsen IK, Jonsdottir KY, Tietze A, Blicher JU, Aamand R, Hjort N, Iversen NK, Cai C, Hougaard KD, Simonsen CZ, Von Weitzel-Mudersbach P, Modrau B, Nagenthiraja K, Riisgaard Ribe L, Hansen MB, Bekke SL, Dahlman MG, Puig J, Pedraza S, Serena J, Cho TH, Siemonsen S, Thomalla G, Fiehler J, Nighoghossian N, Andersen G (2013) The role of the cerebral capillaries in acute ischemic stroke: The extended penumbra model. *J Cereb Blood Flow Metab* **33**, 635-648.

[22] Ostergaard L, Aamand R, Gutierrez-Jimenez E, Ho YC, Blicher JU, Madsen SM, Nagenthiraja K, Dalby RB, Drasbek KR, Moller A, Braendgaard H, Mouridsen K, Jespersen SN, Jensen MS, West MJ (2013) The capillary dysfunction hypothesis of Alzheimer's disease. *Neurobiol Aging* **34**, 1018-1031.

[23] Iadecola C (2010) The overlap between neurodegenerative and vascular factors in the pathogenesis of dementia. *Acta Neuropathol* **120**, 287-296.

[24] Thal DR, Ghebremedhin E, Rub U, Yamaguchi H, Del Tredici K, Braak H (2002) Two types of sporadic cerebral amyloid angiopathy. *J Neuropathol Exp Neurol* **61**, 282-293.

[25] Stankoff B, Freeman L, Aigrot MS, Chardain A, Dolle F, Williams A, Galanaud D, Armand L, Lehericy S, Lubetzki C, Zalc B, Bottlaender M (2011) Imaging central nervous system myelin by positron emission tomography in multiple sclerosis using [methyl-(1)(1)C]-2-(4'-methylaminophenyl)- 6-hydroxybenzothiazole. *Ann Neurol* **69**, 673-680.

[26] Goodheart AE, Tamburo E, Minhas D, Aizenstein HJ, McDade E, Snitz BE, Price JC, Mathis CA, Lopez OL, Klunk WE, Cohen AD (2015) Reduced binding of Pittsburgh Compound-B in areas of white matter hyperintensities. *Neuroimage Clin* **9**, 479-483.

[27] Glodzik L, Rusinek H, Li J, Zhou C, Tsui W, Mosconi L, Li Y, Osorio R, Williams S, Randall C, Spector N, McHugh P, Murray J, Pirraglia E, Vallabhajolusa S, de Leon M (2015) Reduced retention of Pittsburgh compound B in white matter lesions. *Eur J Nucl Med Mol Imaging* **42**, 97-102.

[28] Lockhart A, Lamb JR, Osredkar T, Sue LI, Joyce JN, Ye L, Libri V, Leppert D, Beach TG (2007) PIB is a non-specific imaging marker of amyloid-beta (Abeta) peptide-related cerebral amyloidosis. *Brain* **130**, 2607-2615.

[29] Johnson KA, Gregas M, Becker JA, Kinnecom C, Salat DH, Moran EK, Smith EE, Rosand J, Rentz DM, Klunk WE, Mathis CA, Price JC, Dekosky ST, Fischman AJ, Greenberg SM (2007) Imaging of amyloid burden and distribution in cerebral amyloid angiopathy. *Ann Neurol* **62**, 229-234.

[30] Almdahl IS, Lauridsen C, Selnes P, Kalheim LF, Coello C, Gajdzik B, Møller I, Wettergreen M, Grambaite R, Bjørnerud A, Bråthen G, Sando SB, White LR, Fladby T (2017) Cerebrospinal fluid levels of amyloid beta 1-43 mirror 1-42 in relation to imaging biomarkers of Alzheimer's disease. *Front Aging Neurosci* **9**, 9.

[31] Albert MS, DeKosky ST, Dickson D, Dubois B, Feldman HH, Fox NC, Gamst A, Holtzman DM, Jagust WJ, Petersen RC, Snyder PJ, Carrillo MC, Thies B, Phelps CH (2011) The diagnosis of mild cognitive impairment due to Alzheimer's disease: Recommendations from the National Institute on Aging-Alzheimer's Association workgroups on diagnostic guidelines for Alzheimer's disease. *Alzheimers Dement* **7**, 270-279.

[32] Jessen F, Amariglio RE, van Boxtel M, Breteler M, Ceccaldi M, Chetelat G, Dubois B, Dufouil C, Ellis KA, van der Flier WM, Glodzik L, van Harten AC, de Leon MJ, McHugh P, Mielke MM, Molinuevo JL, Mosconi L, Osorio RS, Perrotin A, Petersen RC, Rabin LA, Rami L, Reisberg B, Rentz DM, Sachdev PS, de la Sayette V, Saykin AJ, Scheltens P, Shulman MB, Slavin MJ, Sperling RA, Stewart R, Uspenskaya O, Vellas B, Visser PJ, Wagner M (2014) A conceptual framework for research on subjective cognitive decline in preclinical Alzheimer's disease. *Alzheimers Dement* **10**, 844-852.

[33] Morris JC (1997) Clinical dementia rating: A reliable and valid diagnostic and staging measure for dementia of the Alzheimer type. *Int Psychogeriatr* **9** Suppl (1), 173-176; discussion 177-178.

[34] Sperling RA, Aisen PS, Beckett LA, Bennett DA, Craft S, Fagan AM, Iwatsubo T, Jack CR Jr, Kaye J, Montine TJ, Park DC, Reiman EM, Rowe CC, Siemers E, Stern Y, Yaffe K, Carrillo MC, Thies B, Morrison-Bogorad M, Wagster MV, Phelps CH (2011) Toward defining the preclinical stages of Alzheimer's disease: Recommendations from the National Institute on Aging-Alzheimer's Association workgroups on diagnostic guidelines for Alzheimer's disease. *Alzheimers Dement* **7**, 280-292.

[35] Coello C, Willoch F, Selnes P, Gjerstad L, Fladby T, Skretting A (2013) Correction of partial volume effect in (18)F-FDG PET brain studies using coregistered MR vol-

umes: Voxel based analysis of tracer uptake in the white matter. *Neuroimage* **72**, 183-192.

[36] Bettinardi V, Presotto L, Rapisarda E, Picchio M, Gianolli L, Gilardi MC (2011) Physical performance of the new hybrid PETCT Discovery-690. *Med Phys* **38**, 5394-5411.

[37] Rincon M, Diaz-Lopez E, Selnes P, Vegge K, Altmann M, Fladby T, Bjornerud A (2017) Improved automatic segmentation of white matter hyperintensities in mri Based on Multilevel Lesion Features. *Neuroinformatics* **15**, 231-245.

[38] Smith SM, Jenkinson M, Woolrich MW, Beckmann CF, Behrens TE, Johansen-Berg H, Bannister PR, De Luca M, Drobnjak I, Flitney DE, Niazy RK, Saunders J, Vickers J, Zhang Y, De Stefano N, Brady JM, Matthews PM (2004) Advances in functional and structural MR image analysis and implementation as FSL. *Neuroimage* **23**(Suppl 1), S208-S219.

[39] Woolrich MW, Jbabdi S, Patenaude B, Chappell M, Makni S, Behrens T, Beckmann C, Jenkinson M, Smith SM (2009) Bayesian analysis of neuroimaging data in FSL. *Neuroimage* **45**, S173-S186.

[40] Desikan RS, Segonne F, Fischl B, Quinn BT, Dickerson BC, Blacker D, Buckner RL, Dale AM, Maguire RP, Hyman BT, Albert MS, Killiany RJ (2006) An automated labeling system for subdividing the human cerebral cortex on MRI scans into gyral based regions of interest. *Neuroimage* **31**, 968-980.

[41] Thal DR, Attems J, Ewers M (2014) Spreading of amyloid, tau, and microvascular pathology in Alzheimer's disease: Findings from neuropathological and neuroimaging studies. *J Alzheimers Dis* **42**(Suppl 4), S421-S429.

[42] (2013) Vizamyl. (Prescribing information). GE Healthcare, Arlington Heights, IL.

[43] Sjogren M, Vanderstichele H, Agren H, Zachrisson O, Edsbagge M, Wikkelso C, Skoog I, Wallin A, Wahlund LO, Marcusson J, Nagga K, Andreasen N, Davidsson P, Vanmechelen E, Blennow K (2001) Tau and Abeta42 in cerebrospinal fluid from healthy adults 21-93 years of age: Establishment of reference values. *Clin Chem* **47**, 1776-1781.

[44] Thurfjell L, Lilja J, Lundqvist R, Buckley C, Smith A, Vandenberghe R, Sherwin P (2014) Automated quantification of 18F-flutemetamol PET activity for categorizing scans as negative or positive for brain amyloid: Concordance with visual image reads. *J Nucl Med* **55**, 1623-1628.

[45] Thal DR, Rub U, Orantes M, Braak H (2002) Phases of A beta-deposition in the human brain and its relevance for the development of AD. *Neurology* **58**, 1791-1800.

[46] Mosconi L (2005) Brain glucose metabolism in the early and specific diagnosis of Alzheimer's disease. FDG-PET studies in MCI and AD. *Eur J Nucl Med Mol Imaging* **32**, 486-510.

[47] Engler H, Forsberg A, Almkvist O, Blomquist G, Larsson E, Savitcheva I, Wall A, Ringheim A, Langstrom B, Nordberg A (2006) Two-year follow-up of amyloid deposition in patients with Alzheimer's disease. *Brain* **129**, 2856-2866.

[48] Cohen AD, Price JC, Weissfeld LA, James J, Rosario BL, Bi W, Nebes RD, Saxton JA, Snitz BE, Aizenstein HA, Wolk DA, Dekosky ST, Mathis CA, Klunk WE (2009) Basal cerebral metabolism may modulate the cognitive effects of Abeta in mild cognitive impairment: An example of brain reserve. *J Neurosci* **29**, 14770-14778.

[49] Li Y, Rinne JO, Mosconi L, Pirraglia E, Rusinek H, DeSanti S, Kemppainen N, Nagren K, Kim BC, Tsui W, de Leon MJ (2008) Regional analysis of FDG and PIB-PET images in normal aging, mild cognitive impairment, and Alzheimer's disease. *Eur J Nucl Med Mol Imaging* **35**, 2169-2181.

[50] Rabinovici GD, Furst AJ, Alkalay A, Racine CA, O'Neil JP, Janabi M, Baker SL, Agarwal N, Bonasera SJ, Mormino EC, Weiner MW, Gorno-Tempini ML, Rosen HJ, Miller BL, Jagust WJ (2010) Increased metabolic vulnerability in early-onset Alzheimer's disease is not related to amyloid burden. *Brain* **133**, 512-528.

[51] Esparza TJ, Zhao H, Cirrito JR, Cairns NJ, Bateman RJ, Holtzman DM, Brody DL (2013) Amyloid-beta oligomerization in Alzheimer dementia versus high-pathology controls. *Ann Neurol* **73**, 104-119.

[52] Hoffman EJ, Huang SC, Phelps ME (1979) Quantitation in positron emission computed tomography: 1. Effect of object size. *J Comput Assist Tomogr* **3**, 299-308.

[53] Matsubara K, Ibaraki M, Shimada H, Ikoma Y, Suhara T, Kinoshita T, Itco H (2016) Impact of spillover from white matter by partial volume effect on quantification of amyloid deposition with [11C]PiB PET. *Neuroimage* **143**, 316-324.

[54] Landau SM, Breault C, Joshi AD, Pontecorvo M, Mathis CA, Jagust WJ, Mintun MA (2013) Amyloid-beta imaging with Pittsburgh compound B and florbetapir: Comparing radiotracers and quantification methods. *J Nucl Med* **54**, 70-77.

[55] Becker GA, Ichise M, Barthel H, Luthardt J, Patt M, Seese A, Schultze-Mosgau M, Rohde B, Gertz HJ, Reininger C, Sabri O (2013) PET quantification of 18F-florbetaben binding to beta-amyloid deposits in human brains. *J Nucl Med* **54**, 723-731.

[56] Selkoe DJ, Hardy J (2016) The amyloid hypothesis of Alzheimer's disease at 25 years. *EMBO Mol Med* **8**, 595-608.

[57] Fernando MS, Simpson JE, Matthews F, Brayne C, Lewis CE, Barber R, Kalaria RN, Forster G, Esteves F, Wharton SB, Shaw PJ, O'Brien JT, Ince PG (2006) White matter lesions in an unselected cohort of the elderly: Molecular pathology suggests origin from chronic hypoperfusion injury. *Stroke* **37**, 1391-1398.

[58] Matías-Guiu JA, Cabrera-Martín MN, Matías-Guiu J, Oreja-Guevara C, Riola-Parada C, Moreno-Ramos T, Arrazola J, Carreras JL (2015) Amyloid PET imaging in multiple sclerosis: An (18)F-florbetaben study. *BMC Neurology* **15**, 243.

[59] Rozemuller AJ, van Gool WA, Eikelenboom P (2005) The neuroinflammatory response in plaques and amyloid angiopathy in Alzheimer's disease: Therapeutic implications. *Curr Drug Targets CNS Neurol Disord* **4**, 223-233.

[60] Zlokovic BV (2011) Neurovascular pathways to neurodegeneration in Alzheimer's disease and other disorders. *Nat Rev Neurosci* **12**, 723-738.

[61] (2013) Amyvid. (Prescribing information). Eli Lilly & Company, Indianapolis, IN.